



CAN UNCLASSIFIED



DRDC | RDDC  
technology science technologie

# Results from off-board noise prediction study in ORCA-class training vessel

Graeme Larsen  
Dalhousie University  
DRDC – Atlantic Research Centre

Jasper Dupuis  
Layton Gilroy  
DRDC – Atlantic Research Centre

The body of this CAN UNCLASSIFIED document does not contain the required security banners according to DND security standards. However, it must be treated as CAN UNCLASSIFIED and protected appropriately based on the terms and conditions specified on the covering page.

**Defence Research and Development Canada**

**Scientific Report**

DRDC-RDDC-2021-R003

January 2021

CAN UNCLASSIFIED

## CAN UNCLASSIFIED

### IMPORTANT INFORMATIVE STATEMENTS

This document was reviewed for Controlled Goods by Defence Research and Development Canada (DRDC) using the Schedule to the *Defence Production Act*.

Disclaimer: This publication was prepared by Defence Research and Development Canada an agency of the Department of National Defence. The information contained in this publication has been derived and determined through best practice and adherence to the highest standards of responsible conduct of scientific research. This information is intended for the use of the Department of National Defence, the Canadian Armed Forces ("Canada") and Public Safety partners and, as permitted, may be shared with academia, industry, Canada's allies, and the public ("Third Parties"). Any use by, or any reliance on or decisions made based on this publication by Third Parties, are done at their own risk and responsibility. Canada does not assume any liability for any damages or losses which may arise from any use of, or reliance on, the publication.

Endorsement statement: This publication has been peer-reviewed and published by the Editorial Office of Defence Research and Development Canada, an agency of the Department of National Defence of Canada. Inquiries can be sent to: Publications.DRDC-RDDC@drdc-rddc.gc.ca.

© Her Majesty the Queen in Right of Canada (Department of National Defence), 2021

© Sa Majesté la Reine en droit du Canada (Ministère de la Défense nationale), 2021

CAN UNCLASSIFIED

## **Abstract**

---

Transport Canada is interested in the real-time estimation of underwater radiated noise based on on-board measurements due to its impact on marine mammals. At Transport Canada's request, Defence Research and Development Canada (DRDC) performed a trial to measure both on-board vibrations and off-board underwater noise produced by an ORCA-class patrol vessel. The post-trial work is a first attempt at adapting real-time acoustic signature estimation procedures that have previously been developed by an international partner (COSIMAR, STEAM and MEASURE trials). Analysis of the trial data shows that it is possible to accurately reconstruct the off-board noise spectrum using few hull and machine-mounted accelerometers. It should also be possible to estimate the cavitation state of the propeller based on the predicted noise levels.

## **Significance to Defence and Security**

---

Successful development of a transfer function relating on-board and off-board noise will assist the transition of this type of system to naval platforms, supporting the development of acoustic signature management systems for the Royal Canadian Navy (RCN).

## Résumé

---

Transports Canada songe à évaluer en temps réel le bruit sous-marin en mesurant les vibrations à bord des navires en raison de leurs effets sur les mammifères marins. À la demande de Transports Canada, Recherche et développement pour la défense Canada (RRDC) a procédé à un essai afin de mesurer les vibrations à bord et le bruit sous-marin produit par un navire de patrouille de la classe ORCA. Les travaux effectués après cet essai constituent une première tentative pour adapter la procédure d'évaluation de la signature acoustique en temps réel élaborée précédemment par un partenaire international (essais de COSIMAR, STEAM et MEASURE). L'analyse des données de l'essai a montré qu'il était possible de reproduire avec exactitude le spectre du bruit sous-marin à l'aide de quelques accéléromètres montés sur la coque et embarqués sur la machine. On devrait également être en mesure d'évaluer l'état de cavitation de l'hélice sur la base des niveaux de bruit prévus.

## Importance pour la défense et la sécurité

---

En parvenant à établir une fonction de transfert entre les vibrations à bord et le bruit sous-marin, on facilitera la transition entre ce type de système et les plates-formes navales, ce qui contribuera à l'élaboration de systèmes de gestion de la signature acoustique pour la Marine royale canadienne (MRC).

# Table of Contents

---

Abstract . . . . .	i
Significance to Defence and Security. . . . .	i
Résumé . . . . .	ii
Importance pour la défense et la sécurité . . . . .	ii
Table of Contents . . . . .	iii
List of Figures . . . . .	v
List of Tables . . . . .	vii
Acknowledgements . . . . .	viii
1 Introduction . . . . .	1
1.1 Ship Specifications . . . . .	1
1.2 Data Acquisition . . . . .	1
1.2.1 On-Board Accelerometer Placement . . . . .	1
1.2.2 Underwater Hydrophone Placement. . . . .	3
1.3 Trial Plan . . . . .	3
1.3.1 Static Ranging . . . . .	3
1.3.2 Dynamic Ranging . . . . .	3
2 Analysis Approach . . . . .	4
2.1 Noise Level Estimation . . . . .	4
2.1.1 Non-Negative Least Squares Method (NNLS) . . . . .	4
2.2 Cavitation Inception Prediction . . . . .	5
3 Pre-Analysis . . . . .	6
3.1 North vs. South Hydrophone Comparison . . . . .	6
3.2 East vs. West Heading Comparison . . . . .	6
3.3 Correlation Between Vibrations and Off-Board Noise . . . . .	7
3.4 Squealing Sound During 11 Knot Runs . . . . .	9
4 Results and Discussion . . . . .	11
4.1 Noise Level Estimation . . . . .	11
4.1.1 Reconstruction With Same Speed and Machine State . . . . .	11
4.1.2 Reconstruction With Same Speed, Different Machine State . . . . .	18
4.1.3 Reconstruction With Different Speeds in Training Runs . . . . .	20
4.1.4 Reconstructing the 11 Knot Squeal . . . . .	22
4.1.5 Keel Runs . . . . .	24
4.2 Cavitation Inception Prediction . . . . .	26
5 Conclusion . . . . .	28
6 Recommendations . . . . .	29
References . . . . .	30

Annex A Dynamic Ranging Run List . . . . . 31  
Annex B Results From Attempted Reconstructions . . . . . 33  
List of Symbols/Abbreviations/Acronyms/Initialisms. . . . . 36

# List of Figures

---

Figure 1:	ORCA-class patrol craft, training [1]. . . . .	1
Figure 2:	Sensor location within ORCA’s engine room [1]. . . . .	2
Figure 3:	North vs. south hydrophone measurement comparison. Y-axis reference is $1\mu\text{Pa}^2/\text{Hz}$ . . . . .	6
Figure 4:	East vs. west heading comparison. Y-axis reference is $1\mu\text{Pa}^2/\text{Hz}$ . . . . .	7
Figure 5:	Correlation between hull vibrations and off-board noise at 250 Hz. Y-axis reference is $1\mu\text{Pa}^2/\text{Hz}$ . . . . .	8
Figure 6:	Correlation between hull vibrations and off-board noise at 8000 Hz. Y-axis reference is $1\mu\text{Pa}^2/\text{Hz}$ . . . . .	8
Figure 7:	Correlation between engine vibrations and off-board noise at 250 Hz. Y-axis reference is $1\mu\text{Pa}^2/\text{Hz}$ . . . . .	9
Figure 8:	Correlation between engine vibrations and off-board noise at 8000 Hz. Y-axis reference is $1\mu\text{Pa}^2/\text{Hz}$ . . . . .	9
Figure 9:	NB and OTO spectrum for 11 knot run, Machine State A. Y-axis reference is $1\mu\text{Pa}^2/\text{Hz}$ . . . . .	10
Figure 10:	Correlation matrix for 5 knot Machine State A runs. . . . .	12
Figure 11:	Error in 5 knot, Machine State A reconstruction. Y-axis reference is $1\mu\text{Pa}^2/\text{Hz}$ . . . . .	12
Figure 12:	Error in 9 knot, Machine State A reconstruction. Y-axis reference is $1\mu\text{Pa}^2/\text{Hz}$ . . . . .	13
Figure 13:	Error in 19 knot, Machine State A reconstruction. Y-axis reference is $1\mu\text{Pa}^2/\text{Hz}$ . . . . .	13
Figure 14:	Actual vs. reconstructed spectrum for 5 knot run with hull sensors. Y-axis reference is $1\mu\text{Pa}^2/\text{Hz}$ . . . . .	13
Figure 15:	Actual vs. reconstructed spectrum for 19 knot run with hull sensors. Y-axis reference is $1\mu\text{Pa}^2/\text{Hz}$ . . . . .	14
Figure 16:	Five knot, Machine State A reconstruction with machine sensors. Y-axis reference is $1\mu\text{Pa}^2/\text{Hz}$ . . . . .	15
Figure 17:	Correlation matrix for 5 knot, Machine State A runs with machine sensors. . . . .	15
Figure 18:	Plot of estimated and actual spectrum, 5 knots. Y-axis reference is $1\mu\text{Pa}^2/\text{Hz}$ . . . . .	16
Figure 19:	Plot of estimated and actual spectra, 9 knots. Y-axis reference is $1\mu\text{Pa}^2/\text{Hz}$ . . . . .	16
Figure 20:	Plot of estimated and actual spectra, 19 knots. Y-axis reference is $1\mu\text{Pa}^2/\text{Hz}$ . . . . .	16
Figure 21:	Correlation matrix for 9 knot, Machine State A runs with machine sensors. . . . .	17
Figure 22:	Correlation matrix for 19 knot, Machine State A runs with machine sensors. . . . .	17
Figure 23:	Reconstructing runs with different machine states (A–H). Y-axis reference is $1\mu\text{Pa}^2/\text{Hz}$ . . . . .	18

Figure 24: Comparison of off-board spectra for two machine states at 5 knots. Y-axis reference is  $1\mu\text{Pa}^2/\text{Hz}$ . . . . . 19

Figure 25: Reconstruction using combination of machine states for training. Y-axis reference is  $1\mu\text{Pa}^2/\text{Hz}$ . . . . . 19

Figure 26: Error for reconstruction of non-cavitating runs with different training speeds. Y-axis reference is  $1\mu\text{Pa}^2/\text{Hz}$ . . . . . 20

Figure 27: Error for reconstruction of cavitating runs with different training speeds. Y-axis reference is  $1\mu\text{Pa}^2/\text{Hz}$ . . . . . 21

Figure 28: Error in 17 knot reconstruction using 15, 17, and 19 knot training runs. Y-axis reference is  $1\mu\text{Pa}^2/\text{Hz}$ . . . . . 21

Figure 29: Error in 9 knot reconstruction using 9, 13, and 15 knot training runs. Y-axis reference is  $1\mu\text{Pa}^2/\text{Hz}$ . . . . . 22

Figure 30: Eleven knot spectrum reconstruction from 9, 13 and 15 knot training runs. Y-axis reference is  $1\mu\text{Pa}^2/\text{Hz}$ . . . . . 23

Figure 31: Hull sensor spectra for 11 knot run. Y-axis reference is  $1\mu\text{Pa}^2/\text{Hz}$ . . . . . 23

Figure 32: Eleven knot spectrum reconstruction when including both stbd sensors. Y-axis reference is  $1\mu\text{Pa}^2/\text{Hz}$ . . . . . 24

Figure 33: Keel vs. beam readings for keel runs. Y-axis reference is  $1\mu\text{Pa}^2/\text{Hz}$ . . . . . 24

Figure 34: Keel vs. beam readings for keel runs after corrections. Y-axis reference is  $1\mu\text{Pa}^2/\text{Hz}$ . . . . . 25

Figure 35: Speed vs. vibration level for the 2.52 kHz bin. Y-axis reference is  $1\text{g}^2/\text{Hz}$ . . . . . 26

Figure 36: Speed vs. vibration level for the 3.17 kHz bin. Y-axis reference is  $1\text{g}^2/\text{Hz}$ . . . . . 26

Figure 37: Approximate cavitation cut-offs for the 2520 Hz bin. Y-axis reference is  $1\mu\text{Pa}^2/\text{Hz}$ . . . . . 27

## List of Tables

---

Table 1:	List of sensors and their locations [1]. . . . .	2
Table 2:	Hydrophone positions at Patricia Bay [1]. . . . .	3
Table 3:	List of machine states for dynamic ranging [1]. . . . .	3
Table A.1:	Dynamic ranging run list. . . . .	31
Table B.1:	Results from attempted reconstructions.. . . . .	33

## **Acknowledgements**

---

The authors would like to acknowledge the Royal Canadian Navy for allowing testing to be conducted aboard their training vessel, as well as DRDC's Sean Kavanaugh, Courtney Greene, Heather Smiley, and Dang Phan for their efforts in collecting the necessary static and dynamic ranging data for the analysis within this Scientific Report.

# 1 Introduction

---

A trial was performed to measure both on-board vibrations and off-board underwater noise for an ORCA-class training vessel available through the Royal Canadian Navy (RCN). Transport Canada is interested in the possible use of this platform to demonstrate how underwater noise from civilian shipping can be controlled, better protecting Canada's southern resident killer whale population located near Vancouver, BC. The project objectives include establishing a baseline acoustic signature level for the vessel, measuring on-board vibrations for correlation with off-board noise levels, and developing a method for cavitation monitoring that can be applied to a variety of ship types. This Scientific Report will consider a method for determining such a correlation, and attempt to show that it can be used to accurately estimate the off-board underwater noise levels. The REPORT will also outline how such an estimation can be used to determine the cavitation state of the ship.

## 1.1 Ship Specifications

The class of vessel under analysis is the ORCA-class training vessel, shown in Figure 1. Built between 2004 and 2008, the ORCAs are operated as training platforms and surveillance craft, and are based at CFB Esquimalt in British Columbia.



*Figure 1: ORCA-class patrol craft, training [1].*

The particular ship under examination is the Patrol Craft Training (PCT) MOOSE. The ship has a length of 33 m, a beam of 8.34 m, a draft of 2.6 m, and a displacement of 210 tons. It is a twin-screw vessel driven by two direct-mounted 2500 HP Caterpillar diesel engines, and has a maximum speed of 20 knots [1].

## 1.2 Data Acquisition

### 1.2.1 On-Board Accelerometer Placement

Defence Research and Development Canada (DRDC) – Atlantic Research Centre installed a 16-channel data acquisition system in the main engine room of PCT MOOSE, and accelerometers were used to measure vibration levels. Four accelerometers were installed on the hull above the propellers, one on each

diesel engine, one on each diesel generator (genset), and one on each of the fire, bilge, and black water pumps for a total of 12 accelerometers. Tachometers were also placed on each propeller shaft to measure the shaft RPM [1]. A list of the sensors and their assigned names can be found in Table 1. An image showing their locations can be seen in Figure 2.

**Table 1:** List of sensors and their locations [1].

Sensor Name	Position
H1	Outboard Prop – Port Side
H2	Inboard Prop – Port Side
H3	Outboard Prop – Stbd Side
H4	Inboard Prop – Stbd Side
M1	Genset – Port Side
M2	Genset – Centre
M3	Genset – Stbd Side
M4	Diesel – Port Side
M5	Diesel – Stbd Side
M6	Fire Pump
M7	Black Water Pump
M8	Bilge Pump

The equipment selected for immediate accelerometer placement are believed to be the major sources of radiated noise not attributable to hydrodynamic effects from the hull or propeller. None of the equipment aboard the ORCA-class vessels is rafted, a common method of machinery noise mitigation.

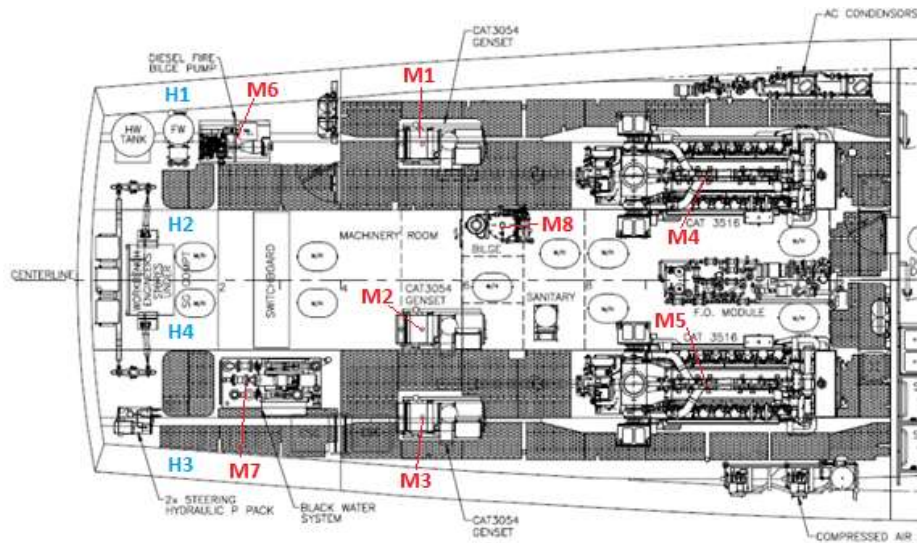


**Figure 2:** Sensor location within ORCA's engine room [1].

## 1.2.2 Underwater Hydrophone Placement

The Patricia Bay acoustic ranging facility is equipped with two hydrophones for dynamic ranging—one to the north, and one to the south. The hydrophone locations are given in Table 2 and a general map is given in Reference [1].

*Table 2: Hydrophone positions at Patricia Bay [1].*

Hydrophone	Latitude	Longitude
North Dynamic Hydrophone	48° 39.550'	123° 28.716'
South Dynamic Hydrophone	48° 39.459'	123° 28.804'

## 1.3 Trial Plan

This section presents a brief summary of the detailed trials plan found in Reference [1].

### 1.3.1 Static Ranging

Static ranging is performed to identify the largest noise contributors aboard the ship, and determine which machine states would be of interest to test. Eight machinery states were identified that were expected to be of interest during the trial [1]. A list of these machine states can be found in Table 3. Note that States G and H involve trailing the indicated propeller (not rotating while the other is propelling the ship).

*Table 3: List of machine states for dynamic ranging [1].*

Machine State	Description
A	Main engines, normal baseline state
B	Main fire pump on
C	Secondary genset
D	Tertiary genset
E	Two gensets
F	Bilge pump on
G	Trail Port Propeller
H	Trail Stbd propeller

### 1.3.2 Dynamic Ranging

In total, 72 dynamic ranging runs were performed, and speed (through engine RPM) and machine state were controlled throughout. Some runs are not useable due to labelling issues resulting in 16 runs being assigned the same identifiers. There are therefore 56 dynamic runs available. A complete list of used dynamic runs and their descriptions can be found in Annex A, including the associated run numbers which will be referenced throughout this Report.

## 2 Analysis Approach

---

### 2.1 Noise Level Estimation

In an attempt to follow previous work by TNO, DRDC's counterpart in the Netherlands, this Report will use the method of non-negative least squares (NNLS). In this method, a set of training runs is used to produce a correlation matrix relating the on-board and off-board data [2]. To verify its effectiveness in estimating off-board noise, this matrix will then be applied to a set of test runs, and the error between the actual noise spectrum for each run and the reconstructed spectrum will be calculated. Error between the actual and estimated spectra will provide insight into how accurate an estimate can be made for the off-board noise level, and will aid in determining the validity of this method.

#### 2.1.1 Non-Negative Least Squares Method (NNLS)

The effectiveness of the NNLS method has previously been examined in a report by TNO using data from a larger RCN vessel, HCMS GLACE BAY. TNO found that applying this method to groups of sensors placed directly on the hull allows for accurate reconstruction of the off-board spectrum [2].

The NNLS method involves creating a weighting matrix that relates the one-third octave (OTO) bins from each sensor to those of the measured off-board spectrum. This allows the system to take into account which sensors/machines have the greatest contribution to the underwater noise in each frequency bin. Note that the one-third octave spectrum was used instead of the narrowband in order to decrease calculation time. The calculations used to determine the correlation vector for each sensor are shown below [2]:

For the  $i^{\text{th}}$  OTO bin, with  $j$  sensors and  $n$  runs:

$$\begin{bmatrix} h_{i1} \\ \vdots \\ h_{in} \end{bmatrix} = \begin{bmatrix} s_{1i1} & \cdots & s_{ji1} \\ \vdots & \ddots & \vdots \\ s_{1in} & \cdots & s_{jin} \end{bmatrix} \begin{bmatrix} \omega_{1i} \\ \vdots \\ \omega_{ji} \end{bmatrix} \quad (1)$$

$$\omega_{ji} = \min_{\omega_{ji}} \left\| s_{jin} \cdot \omega_{ji} - h_{in} \right\|_2^2, \omega_{ji} \geq 0 \quad (2)$$

where:

$h_{in}$  is the hydrophone spectral power for the  $i^{\text{th}}$  bin and  $n^{\text{th}}$  training run,

$s_{jin}$  is the  $j^{\text{th}}$  accelerometer's spectral power for the  $i^{\text{th}}$  bin and  $n^{\text{th}}$  training run,

$\omega_{ji}$  is the weighting value for the  $i^{\text{th}}$  bin and  $j^{\text{th}}$  accelerometer.

When found for each OTO bin, the resulting vectors can be concatenated to form a matrix,  $C$ , which can then be applied to one of the test runs in an attempt to reconstruct the off-board noise spectrum. The

resulting correlation matrix takes the following form where, again,  $\omega_{ji}$  is the weighting value for the  $i^{\text{th}}$  bin and  $j^{\text{th}}$  accelerometer.

$$C = \begin{bmatrix} \omega_{11} & \cdots & \omega_{j1} \\ \vdots & \ddots & \vdots \\ \omega_{1i} & \cdots & \omega_{ji} \end{bmatrix} \quad (3)$$

It should be noted that when used to predict the spectrum for a given run, this correlation is not taken as a matrix, but is instead broken back up into individual vectors that are then applied to the sensor values in each OTO bin.

The NNLS computational problem is solved with Python's SciPy toolkit [3] leveraging a FORTRAN solver developed by Lawson and Hanson [4].

## 2.2 Cavitation Inception Prediction

Using the same vibration measurements, it could also theoretically be possible to estimate the cavitation state of the vessel. Leggat has shown that cavitation produces significant broadband noise beginning at 100 Hz [5]. Above 100 Hz, noise in each OTO bin should be fairly constant until cavitation inception, and then should increase steadily as greater speeds lead to different and louder types of cavitation [5]. A similar trend should also be evident in the vibrations measured by the hull sensors above the propellers.

For each sensor and for each OTO bin, there is a representative accelerometer measurement value and associated ship's speed in the water. This Report uses each OTO bin's mean value over the entire run. Speed is known from notes made on the bridge while conducting each run. These run-wise mean and speed values are then plotted against one another for each sensor and OTO bin. To be clear, there are over 30 such plots for a given sensor.

If cavitation can be predicted from only on-board vibration data, then in some or all of these plots there will be some feature discernible around the known cavitation inception speed. The cavitation inception speed for MOOSE is known from repeated observations made by trial staff listening to range hydrophones in real time. The exact feature will be discussed in Section 4.2.

## 3 Pre-Analysis

### 3.1 North vs. South Hydrophone Comparison

To simplify analysis, it is desirable to use only a single hydrophone, and it is therefore important to know how the measurements from the two hydrophones compare. The north and south spectra for four 5 knot runs in Machine State A are shown in Figure 3.

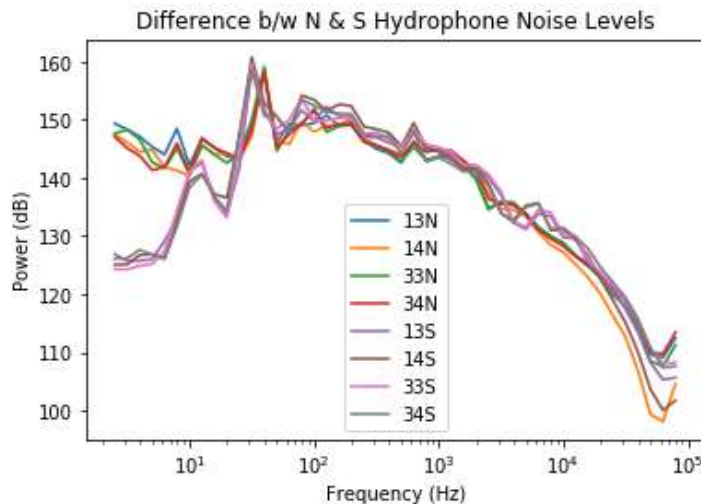


*Figure 3: North vs. south hydrophone measurement comparison. Y-axis reference is  $1\mu\text{Pa}^2/\text{Hz}$ .*

This plot shows that the spectra for the two hydrophones are very similar for frequencies above about 30 Hz. The discrepancy below 30 Hz is ascribed to substantial transmission loss differences, and therefore those values are not used in this Report. Therefore, it can be said that the north and south spectra are similar enough that they do not need to be analyzed separately. Thus, for the purposes of this Report, the measurements taken from one of the hydrophones will suffice, and results can be assumed to be the same as if the other hydrophone were used or if the two were averaged in some fashion. The north hydrophone was arbitrarily selected for use in all tests to ensure consistency.

### 3.2 East vs. West Heading Comparison

It is also important to ensure that the heading of the ship will not have a significant effect on the hydrophone readings, especially at speeds around cavitation inception where ocean currents may play a role. To verify this, the spectra of runs with similar speeds in opposite directions are plotted and observed for any differences. The result for 9 knot runs with Machine State A are displayed in Figure 4. Note that odd run numbers indicate an eastward heading, and even run numbers indicate a westward heading.

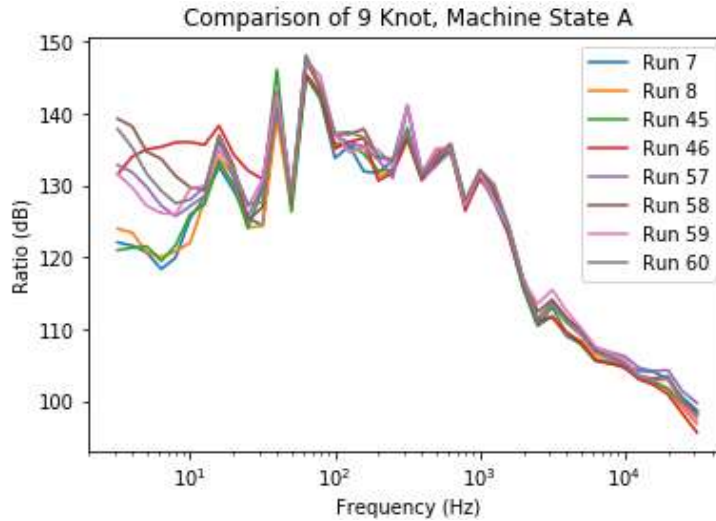


**Figure 4:** East vs. west heading comparison. Y-axis reference is  $1\mu Pa^2/Hz$ .

As Figure 4 shows, for frequencies over about 30 Hz, there is little difference between runs in the same state in opposite directions. Therefore, for the purposes of this Report, runs in the east and west directions can be considered the same, essentially doubling the amount of training data that is available for each speed and machine state.

The findings in this section and the previous section validate the assumption that the vessel acts as a point source for noise in the far-field above 30 Hz, given that hydrophone and aspect performance were identical for runs in different directions.

### 3.3 Correlation Between Vibrations and Off-Board Noise

The off-board noise levels are plotted against the on-board vibrations for different sensors as speed changes, and the correlation levels are investigated. The plots for the hull sensor correlation at 250 Hz and at 8000 Hz are shown in Figures 5 and 6. Because the hull sensors were mounted on the same frame over the propellers, the correlation with off-board noise is the same for all four sensors.

There is a correlation between vibrations in the hull and the off-board noise level, and this correlation increases with frequency. At 250 Hz, the  $R^2$  value is calculated to be 0.88, and at 8000 Hz it is found to be 0.96. To put these values into perspective,  $R^2$  values of 0.75 or greater are considered to show a substantial correlation [6]. It should be noted that even in the 8000 Hz plot, there appears to be more scattering between points at lower noise levels than at higher ones. This will be important moving forward, as it will lead to an increase in error for estimates at lower frequencies.

A similar set of correlations were attempted for the various machine sensors, but it was found that they had little correlation due to the independence of each machine's vibration levels. Since vibrations between machines of different types are not always comparable, it does not make sense to compare them in the same way as the hull sensors. Instead, each machine was analyzed separately, and a significant correlation was again observed. As an example, the correlations between M4 engine vibrations and the off-board noise at 250 Hz and 8000 Hz are displayed in Figures 7 and 8, respectively. Again, greater

correlation is seen at higher frequencies, with an  $R^2$  value of 0.76 at 250 Hz and 0.91 at 8000 Hz. The same trend is seen for all machine sensors.

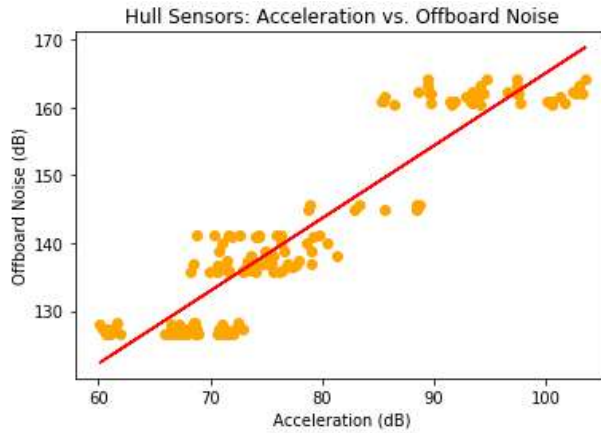


**Figure 5:** Correlation between hull vibrations and off-board noise at 250 Hz. Y-axis reference is  $1\mu Pa^2/Hz$ .

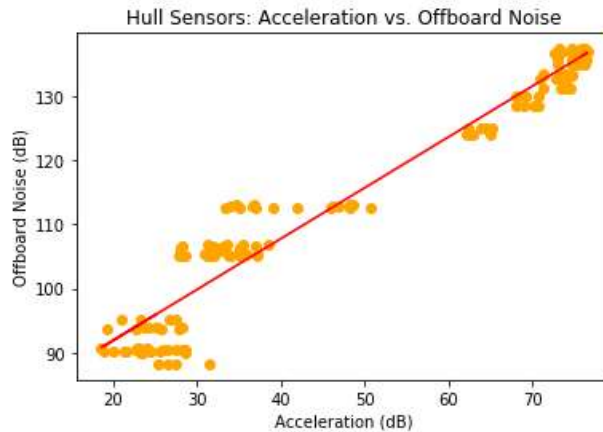


**Figure 6:** Correlation between hull vibrations and off-board noise at 8000 Hz. Y-axis reference is  $1\mu Pa^2/Hz$ .

Because a strong correlation exists between on-board hull vibrations and off-board noise levels, it should be possible to develop an accurate mathematical relationship between the two that can be used in a signature management system. Since a higher correlation exists at higher frequencies, estimates at such frequencies should prove to produce less error. This will be important, as it may be beneficial to focus more strongly on these frequencies for predicting the cavitation state, as it will allow for greater certainty in the prediction.

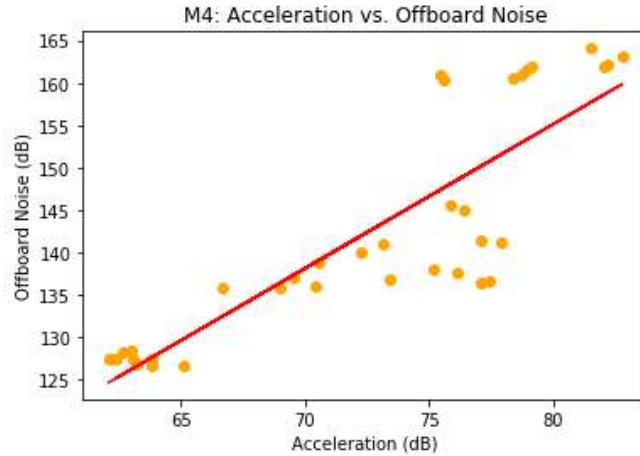


**Figure 7:** Correlation between engine vibrations and off-board noise at 250 Hz. Y-axis reference is  $1\mu Pa^2/Hz$ .

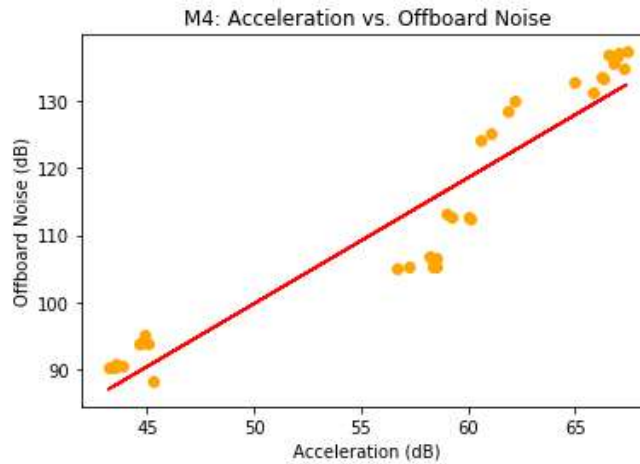


**Figure 8:** Correlation between engine vibrations and off-board noise at 8000 Hz. Y-axis reference is  $1\mu Pa^2/Hz$ .

### 3.4 Squealing Sound During 11 Knot Runs

During the trials, DRDC and range staff observed a loud squealing sound in the runs performed at 11 knots. This sound is apparent in the off-board spectra for the 11 knot runs, shown in Figure 9, as there exists a large peak at 1443 Hz (NB signifies narrow band).

It is hypothesized that this noise was produced by a propeller shaft bearing. This oddity provides an interesting test case. It enables evaluating the effectiveness of correlation methods when unexpected noise sources are present which were not considered in any training runs.

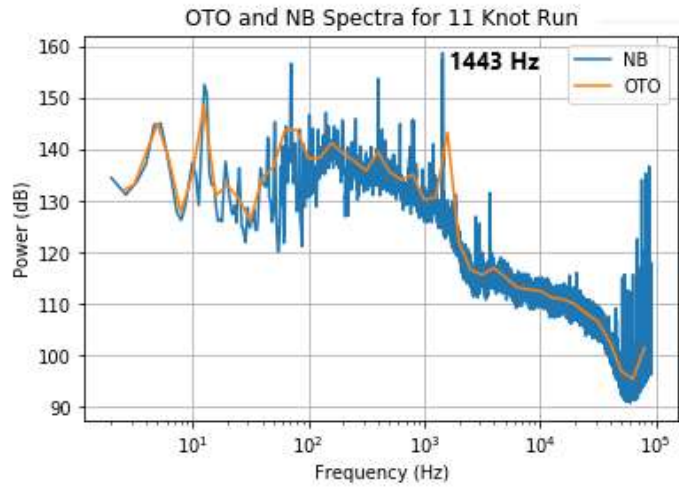


**Figure 9:** NB and OTO spectrum for 11 knot run, Machine State A. Y-axis reference is  $1\mu\text{Pa}^2/\text{Hz}$ .

## 4 Results and Discussion

---

The dataset can be used to test the effectiveness of the NNLS correlation method, and to determine to what degree of accuracy the off-board spectrum can be predicted using on-board vibration measurements. Investigation will also be made into how the reconstructed spectra can be used to predict the cavitation state of the propellers.

### 4.1 Noise Level Estimation

#### 4.1.1 Reconstruction With Same Speed and Machine State

The first step in the analysis is to determine if it is possible to reconstruct the off-board spectrum from the measured on-board vibrations. To do this, runs at 5 knots (non-cavitating), 9 knots (cavitating), 19 knots (cavitating) were examined in Machine State A. These three test cases were selected for this first test due to the large availability of trial data for each. Using the data collected at each speed, correlation matrices were created using a variety of sensor combinations and were applied to test runs of the same speed in an attempt to reconstruct the off-board spectrum.

The correlation matrix for the 5 knot runs in Machine State A using only hull sensors is displayed in Figure 10 in the form of a heat map, for reference (with the weighting constant  $W$  as the scale). Note that the scale represents the ratio between the measured off-board data and the on-board vibration levels, in dB.

In Section 3.3, it was stated that the hull sensors all had the same correlation performance over the entire trial's data set. The heat map in Figure 10 might suggest otherwise when comparing H3 to other sensors. While the correlation of a single on-board sensor with off-board data might be high, it does not follow that a given set of on-board sensors have similar performance over the entire trial. Indeed, it will be seen that an "all-in-one" correlation matrix, derived from cavitating and non-cavitating states, performs less well than matrices derived for their own regions of operation.

The reconstructed spectrum is then compared to the measured off-board spectrum to determine its accuracy. The relevant data produced from this process is shown in Annex B.

Initial results indicate that using only hull-mounted sensors in the correlation matrix, as was done in previous tests conducted by TNO, does not allow for effective reconstruction of the off-board spectrum in all cases. For the 5 knot runs, using only hull-mounted sensors around the propellers, an average error of 2.63 dB was seen above 30 Hz, with a maximum error of 15.9 dB. A plot depicting the error in each bin for this reconstruction can be seen in Figure 11.

In the higher frequencies of each 5 knot reconstruction, significant variability is observed. As speed increases, the reconstruction using only hull sensors becomes more accurate. For 9 and 19 knot reconstructions, the average error for frequencies above 30 Hz drops to 1.43 dB and 0.89 dB respectively, and the maximum error falls to just 4.82 dB for 9 knot runs and 5.19 dB for 19 knot runs. Error plots for these 9 and 19 knot reconstructions can be found in Figures 12 and 13, respectively.

To put these error plots into perspective, the actual and reconstructed spectra are shown in Figures 14 and 15 for a 5 knot and 19 knot run. As these plots show, error of 2.5 dB or less, as seen in the 19 knot plot, results

in a very good prediction of the spectrum. Even error within 5 dB, as seen in the middle frequencies of the 5 knot plot, could be acceptable. However, as the frequency increases in the 5 knot plot, the difference between the actual and estimated spectra becomes much greater than 5 dB, and therefore this result will not be acceptable for radiated noise estimate, as it is no longer representative of the real noise level at these frequencies.

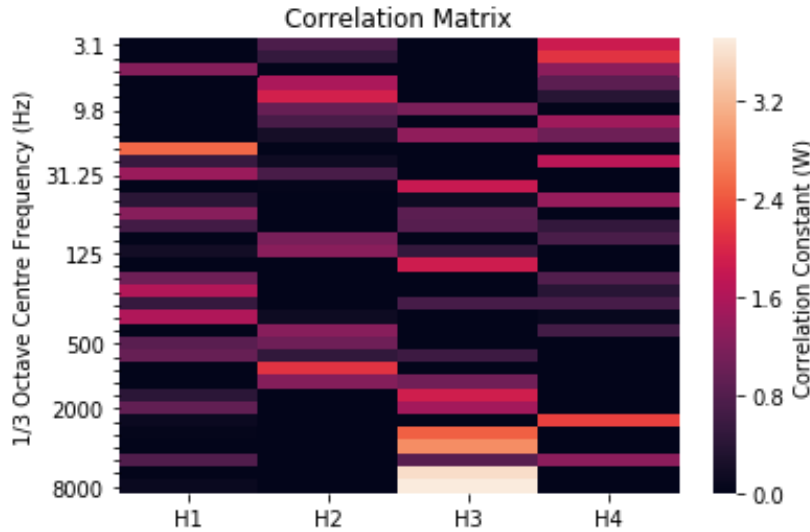


**Figure 10:** Correlation matrix for 5 knot Machine State A runs.

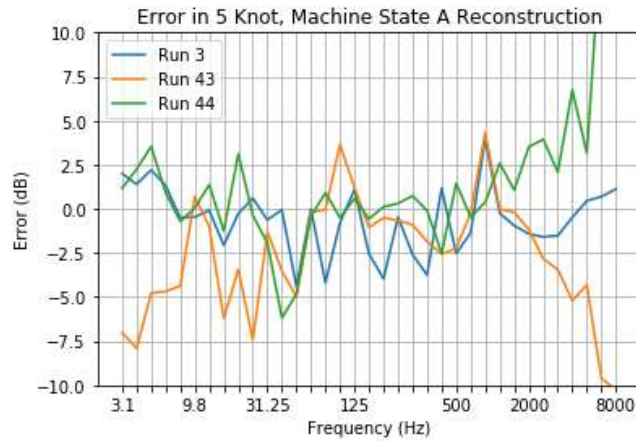


**Figure 11:** Error in 5 knot, Machine State A reconstruction. Y-axis reference is  $1\mu Pa^2/Hz$ .

The improvement in the estimate as speed increases in this case is likely because propeller noise may not be the dominant noise source at speeds below cavitation. Therefore, the measurements from the hull-mounted sensors near the propellers will not be reflective of the actual noise level of the ship at such speeds. However, after cavitation inception, the propellers become the dominant noise source. At this point, the hull-mounted sensor readings will provide a more accurate depiction of the overall noise level of the vessel and the reconstruction will therefore be more accurate.

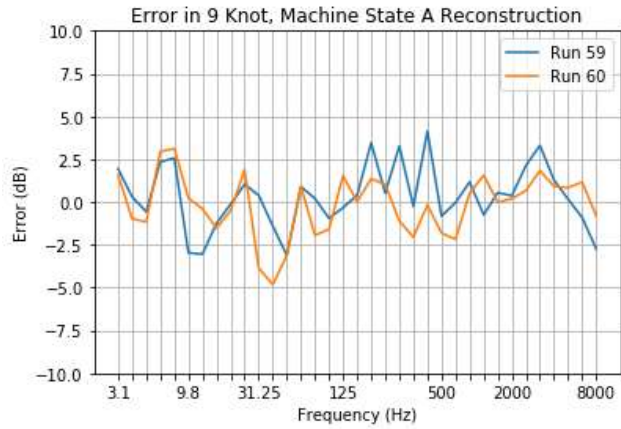


**Figure 12:** Error in 9 knot, Machine State A reconstruction. Y-axis reference is  $1\mu\text{Pa}^2/\text{Hz}$ .

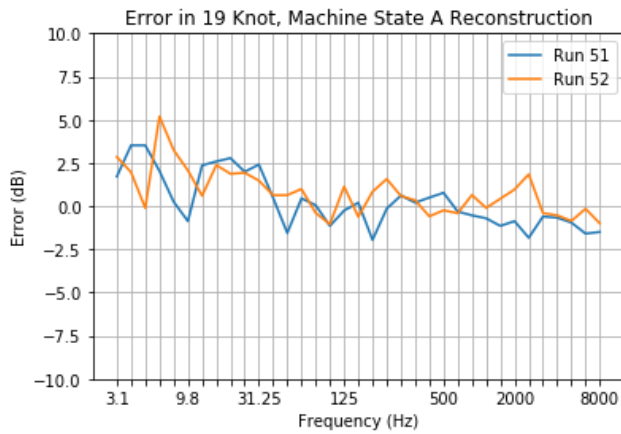


**Figure 13:** Error in 19 knot, Machine State A reconstruction. Y-axis reference is  $1\mu\text{Pa}^2/\text{Hz}$ .

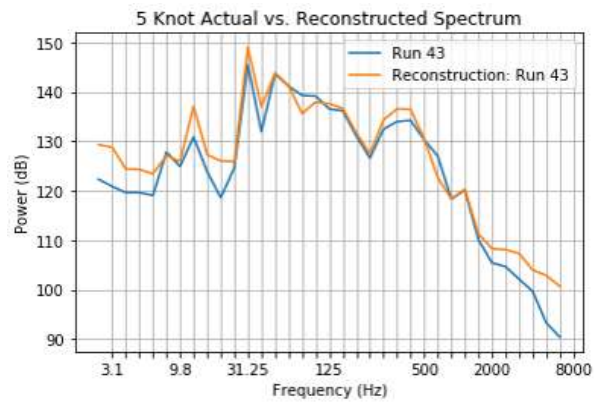


**Figure 14:** Actual vs. reconstructed spectrum for 5 knot run with hull sensors. Y-axis reference is  $1\mu\text{Pa}^2/\text{Hz}$ .

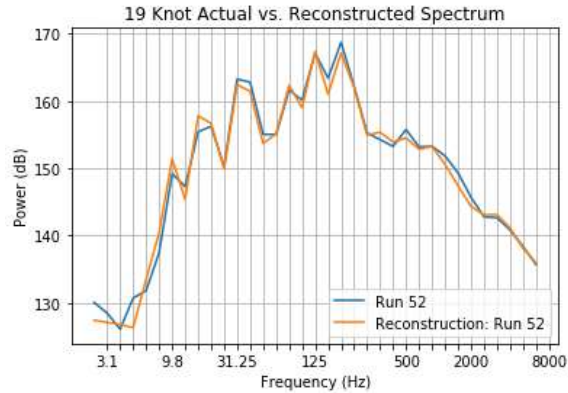


**Figure 15:** Actual vs. reconstructed spectrum for 19 knot run with hull sensors. Y-axis reference is  $1\mu\text{Pa}^2/\text{Hz}$ .

The results found in Annex B also show that there is little difference between using two hull sensors (either inboard or outboard) and using four hull sensors. This means that the use of many hull sensors in a signature management system is likely redundant, and should therefore be avoided to reduce costs.

It is also necessary to investigate how important it is to include machine vibrations in the correlation. Previous analyses [2] have excluded them completely, with the theory that most noise will radiate through the hull into the water and therefore only hull sensors are necessary. Although this was the case for higher speeds in this trial, it was shown to be untrue for slower speeds, as Figure 12 illustrated. This could also be due to the placement of the hull sensors, as all four were located in the aft of the ship. It is possible that placing more hull sensors around other machinery, such as the engines, would allow the system to better account for the noise they produce while still only taking vibration measurements from the hull. This should be considered in future tests, as it would allow for more general sensor placement if one hull sensor could be conveniently placed near several machines instead of having an accelerometer on each individual machine. Because no such sensors were included in this trial, it is impossible to test this theory using the current dataset, and therefore the inclusion of different machine sensors will be considered instead.

Because the machinery on-board PCT MOOSE is quite loud, it was hypothesized that the inclusion of machine sensors in the correlation matrix would improve the reconstruction, especially at lower speeds where propeller noise is less dominant. Results from the reconstruction show that this is, in fact, the case.

When the measurements from the engine sensors are added, a decrease in average error is observed. Figure 16 shows the error in the 5 knot reconstruction after including the active genset's sensor along with the sensor from each engine in the correlation matrix. Figure 17 shows the heat map of this correlation matrix.

As Figure 16 shows, the inclusion of machine sensors in the 5 knot reconstruction effectively eliminates the spreading seen in the previous reconstruction of these runs. In this test, the average error for frequencies above 30 Hz falls to just 1.42 dB, with the maximum error being 4.46 dB. Although less pronounced, the same can be seen in 9 and 19 knot reconstructions, where the average error drops to 1.07 dB and 0.79 dB respectively when machine sensors are included. Plots depicting the actual spectrum vs. the reconstructed spectrum for all three of these speeds can be seen in

Figures 18, 19, and 20, providing an idea of how precise these estimates actually are when the machine sensors are considered as well.

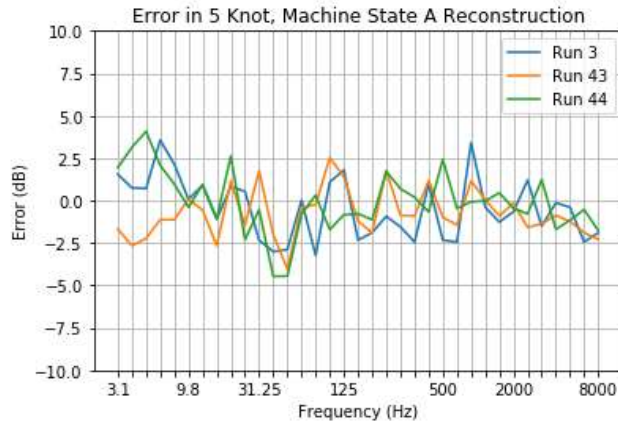


**Figure 16:** Five knot, Machine State A reconstruction with machine sensors. Y-axis reference is  $1\mu\text{Pa}^2/\text{Hz}$ .

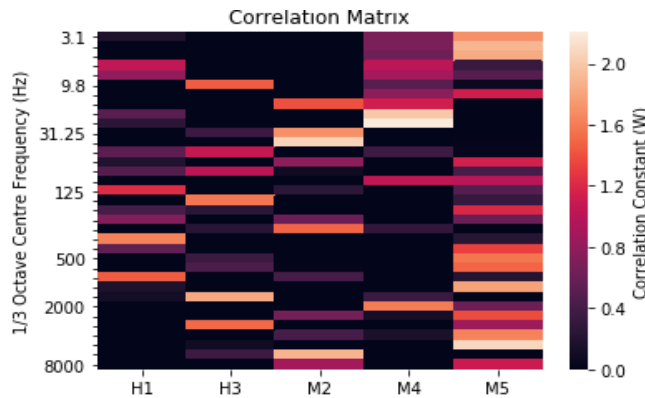


**Figure 17:** Correlation matrix for 5 knot, Machine State A runs with machine sensors.

A look at the correlation heat map for these reconstructions provides a visual indication of why such an improvement is seen in the 5 knot runs, and why it is less pronounced in the higher speed runs. Using only hull sensors, the heat map for the 5 knot runs—seen earlier in Figure 10—showed a fairly even spread of the weighting between all sensors, except at higher frequencies where H3 dominated. In Figure 17, however, the hull sensors receive relatively little weighting compared to the machine sensors. This suggests that at slower speeds, the machine noise is far more dominant than the noise from the propellers, and therefore the inclusion of the machine measurements becomes vital at lower speeds. For comparison, the heat maps for the correlations at 9 and 19 knots for the same machine state are shown in Figures 21 and 22.

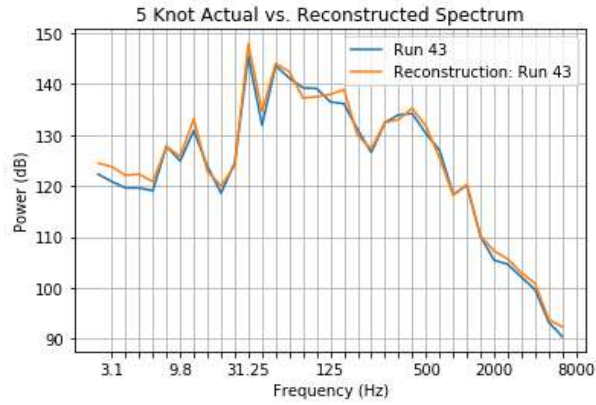


**Figure 18:** Plot of estimated and actual spectrum, 5 knots. Y-axis reference is  $1\mu Pa^2/Hz$ .

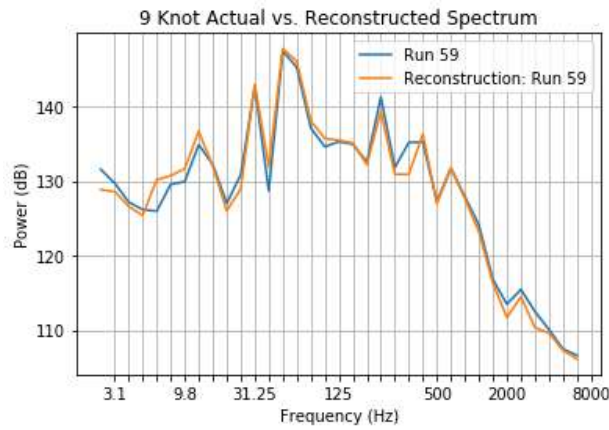


**Figure 19:** Plot of estimated and actual spectra, 9 knots. Y-axis reference is  $1\mu Pa^2/Hz$ .

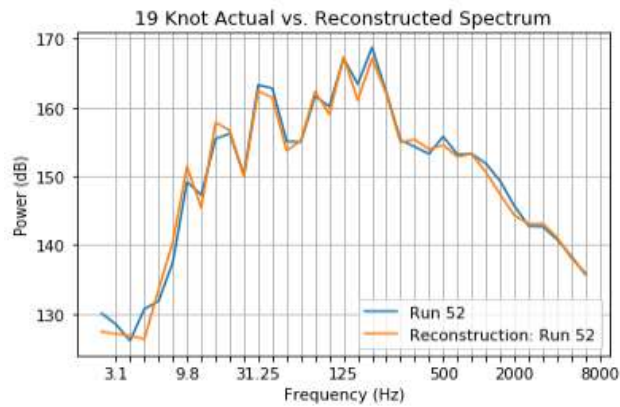


**Figure 20:** Plot of estimated and actual spectra, 19 knots. Y-axis reference is  $1\mu Pa^2/Hz$ .

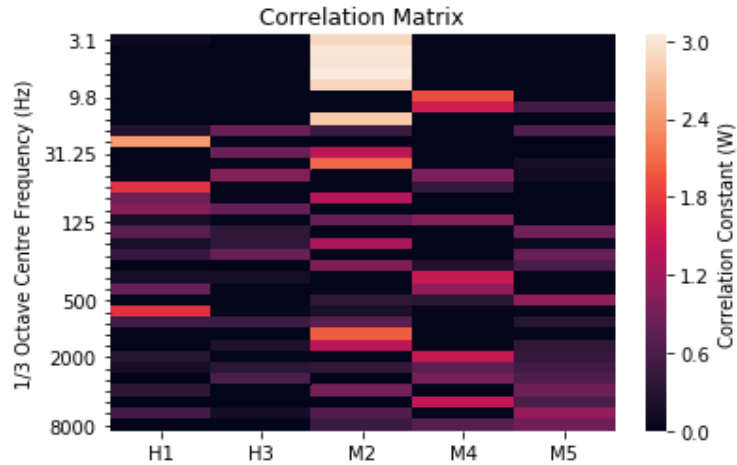


**Figure 21:** Correlation matrix for 9 knot, Machine State A runs with machine sensors.

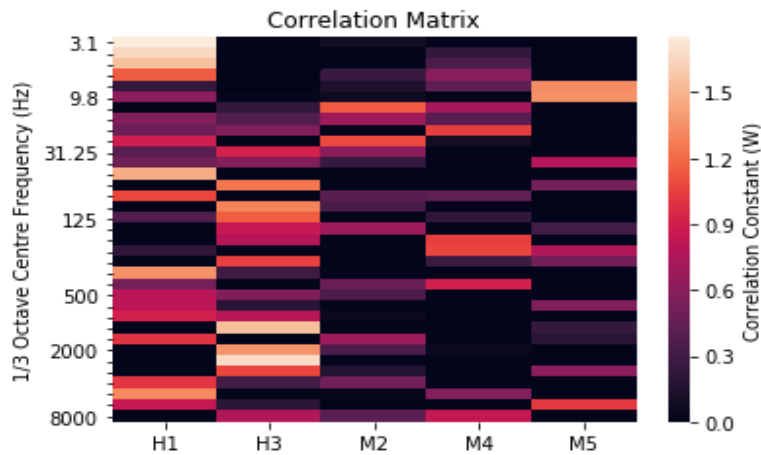


**Figure 22:** Correlation matrix for 19 knot, Machine State A runs with machine sensors.

These graphics show that as speed increases, so too does the weighting assigned to the hull sensors in the heat map. This observation provides further evidence that propeller noise dominates the noise levels above cavitation, and shows why reconstruction when using only hull sensors works better at higher speeds. Looking back, this could also be seen in the correlation between on-board and off-board noise for the hull sensors in Figures 5 through 8, as there exists greater scattering in the lower noise levels (lower speeds) than in the higher noise levels (higher speeds), meaning the hull sensors provide a better picture of the overall noise when the vessel is moving faster. It should be noted that adding machine sensors to the correlation at higher speeds did still increase the accuracy of reconstruction, as it meant more of the noise was accounted for, even if the machines were no longer the dominant noise source.

Overall, the initial results suggest that it is possible to make an accurate estimate of a ship's noise levels using a limited number of sensors, provided that the largest noise contributors are covered by these sensors. The next sections will further investigate the effects of different machine states on the

reconstruction, and the possibility of reducing the number of necessary matrices by using training runs of various speeds, amongst other things.

#### 4.1.2 Reconstruction With Same Speed, Different Machine State

Although it has been shown that it is theoretically possible to reconstruct the far field noise spectrum of a ship from vibration measurements taken in the engine room, there are several variables that affect the accuracy. One such variable is the machine state. Using the correlation matrix for Machine State A using 5 knot runs with two hull sensors, two engine sensors, one genset sensor, and the three pump sensors, the noise spectrum for different machine states was recreated, and the error was examined for each. The resulting error plot is shown in Figure 23.

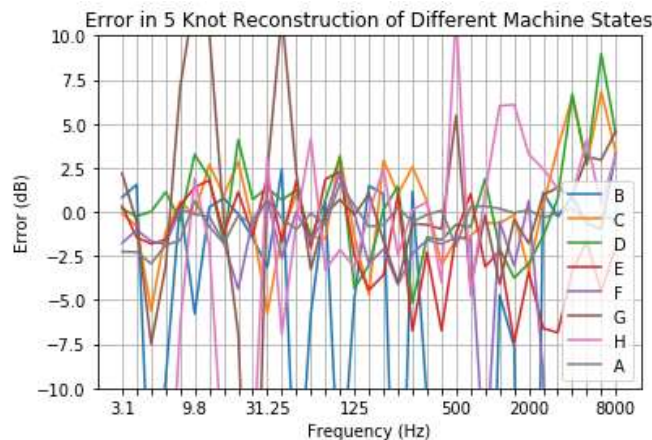


**Figure 23:** Reconstructing runs with different machine states (A–H). Y-axis reference is  $1\mu\text{Pa}^2/\text{Hz}$ .

As this plot shows, the use of a correlation matrix created using runs of a different machine state than the test run leads to lower accuracy in the test run’s reconstructed spectrum, compared to that of a test run with the same machine state as the training runs. In the plot, we see that certain states, namely B, G, and H, reach peak error of over 10 dB in many frequency bins. This is likely a result of the correlation matrix failing to weight sensors properly.

Static ranging tests show that the fire pump is very loud, and therefore will contribute significantly to the ship’s noise level when in operation [7]. This is also seen in the dynamic runs, as analysis of the off-board spectra from State A and State B runs shows that the fire pump adds as much as 15 dB to some OTO bins. This difference is shown in Figure 24, where Run 4 is the State A run and Run 21 is the State B run. In the creation of the correlation matrix from the State A runs, however, the fire pump is turned off, and therefore its sensor receives very little weighting. When the matrix is then applied to a run where the pump is on, its noise is not accounted for properly and the matrix misjudges the amount of noise that it produces.

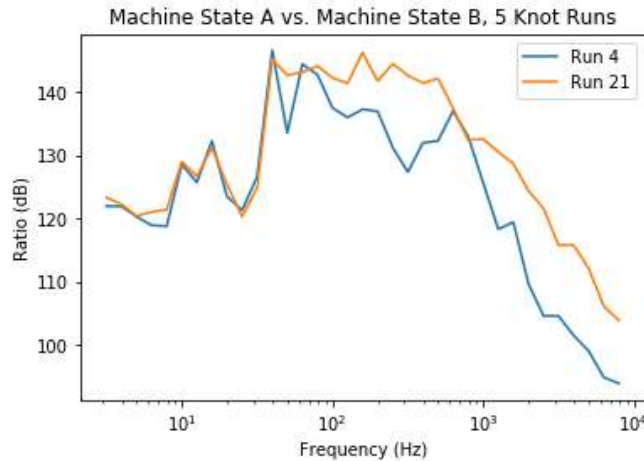


**Figure 24:** Comparison of off-board spectra for two machine states at 5 knots. Y-axis reference is  $1\mu\text{Pa}^2/\text{Hz}$ .

It is possible that including different machine states in the training runs will improve these results by adding weight to the different sensors that were previously unaccounted for. This will likely cause an increase in error in the reconstruction of State A runs that were previously proven to be very accurate, as the matrix will no longer be tailored to that one specific state. In the next test, the matrix is instead constructed using one run at 5 knots from each machine state, and is again applied to test runs from each machine state. The resulting error plot is shown in Figure 25.

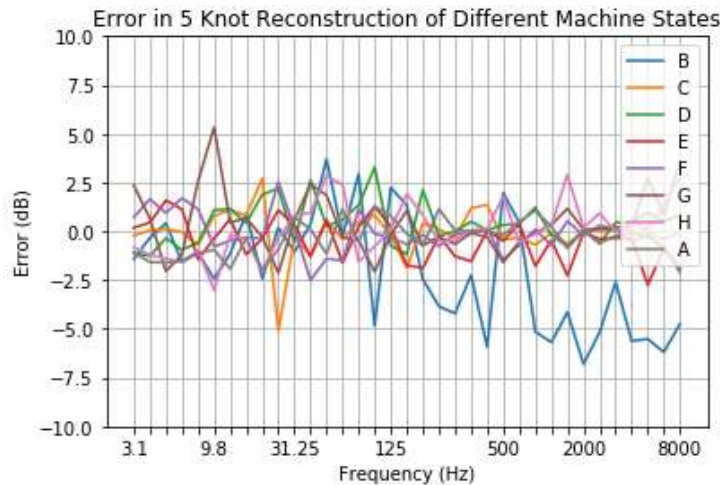


**Figure 25:** Reconstruction using combination of machine states for training. Y-axis reference is  $1\mu\text{Pa}^2/\text{Hz}$ .

The inclusion of multiple machine states in the training runs improved the average reconstruction error across all machine states considerably. Using only State A runs, the maximum error for any machine state was as high as 15 dB, however when using a combination of runs, the maximum error falls to 6.8 dB, and the average error between all reconstructions falls to just 1.16 dB. Therefore, when developing a signature prediction system, it will be important to consider the range of possible machine states for the vessel, and to incorporate these different possible states in the development of any correlation matrix, as was done in

this test. This highlights the importance of static ranging in any range test, as it remains the best method for determining which machines are significant contributors to the ship's signature.

Machine States C, D, E, and F were able to be accurately reconstructed using only training runs from Machine State A. This means that these states are fairly similar to State A, and that the added machinery in these states does not cause a significant change in noise levels. It will be important to consider which machine states are similar in order to minimize the number of sensors in the system by removing those mounted to less significant noise contributors.

### 4.1.3 Reconstruction With Different Speeds in Training Runs

So far, reconstruction has only been attempted on runs with the same speed as those used to create the correlation matrix. It is important, however, to understand how reconstruction will be affected if the training runs are composed of a variety of speeds, as this will allow a signature management system to reduce the number of correlation matrices that it must store.

With machine state held constant, a matrix for the non-cavitating case was created using 3, 5 and 7 knot runs. The resulting error in the reconstruction is shown in Figure 26.

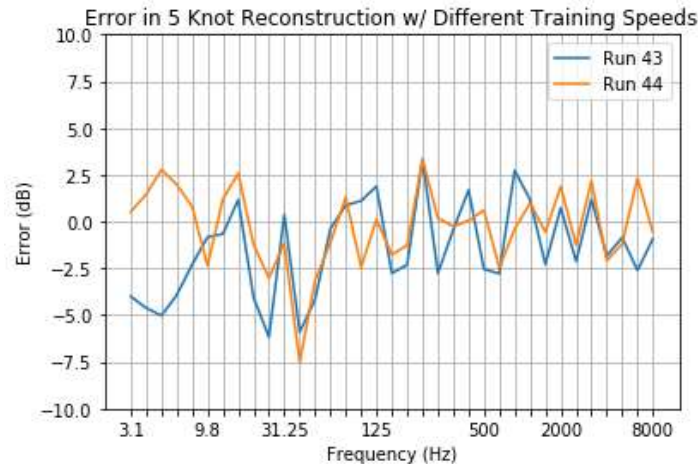


**Figure 26:** Error for reconstruction of non-cavitating runs with different training speeds. Y-axis reference is  $1\mu Pa^2/Hz$ .

For the non-cavitating case, it is possible to reconstruct a fairly accurate spectrum using a combination of speeds in the training set. In this reconstruction, the average error between the real and reconstructed spectra was 1.93 dB, with a maximum error of 7.54 dB occurring around 40 Hz. Better accuracy is evident in the higher frequency bins, as the maximum error never exceeds 3 dB for bins above 50 Hz. Similar results were observed for reconstructions of 3 knot and 7 knot runs.

For the cavitating case, the reconstruction using a variety of speeds during training resulted in significant error in the estimated spectrum. As shown in Figure 27, when an equal number of runs from each speed is used to create the correlation matrix, reconstruction of 9 knot runs results in error exceeding 10 dB in several lower frequency bins, and consistent error of greater than 5 dB at higher frequencies. These errors are likely a result of the large non-linear increase in power in each bin as speed increases, which will be

examined later in this Report. This increase makes it difficult to use higher speed cavitating runs to predict the noise levels of lower speed cavitating runs, as the noise levels will be very different and the correlation will have a tendency to overestimate the noise level for slower speeds, as is the case in Figure 27.

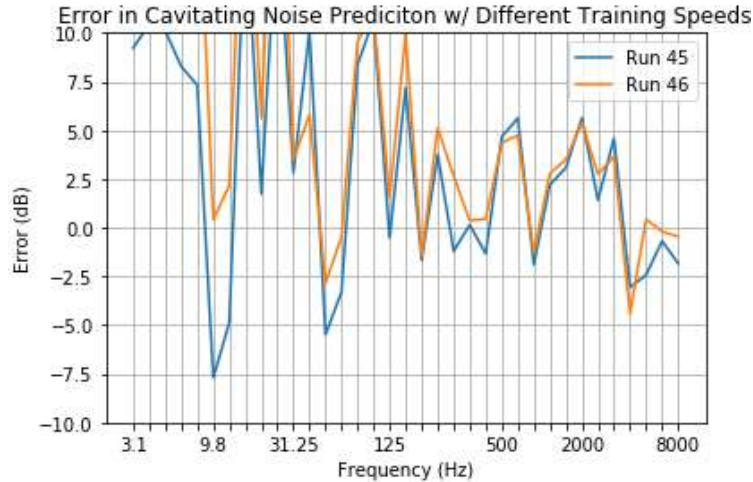


**Figure 27:** Error for reconstruction of cavitating runs with different training speeds. Y-axis reference is  $1\mu\text{Pa}^2/\text{Hz}$ .

Because error of this magnitude will not be acceptable in a signature management system, it is clear that the use of one matrix for all speeds above cavitation will not be possible. It was found, however, that by splitting this range of speeds in two, it is possible to create a more accurate reconstruction for each speed. In this case, the first matrix will be comprised of speeds from 9 knots to 15 knots, and the second of speeds from 15 knots to 20 knots. Note that 11 knot runs are left out of the former, as the added noise in these runs, as discussed in Section 3.4, causes the results to worsen when they are included. The ability of the matrix to reconstruct these 11 knot runs will be examined further in Section 4.1.2. The resulting error plots for reconstruction using the lower and higher speed matrices are displayed in Figures 28 and 29, respectively.

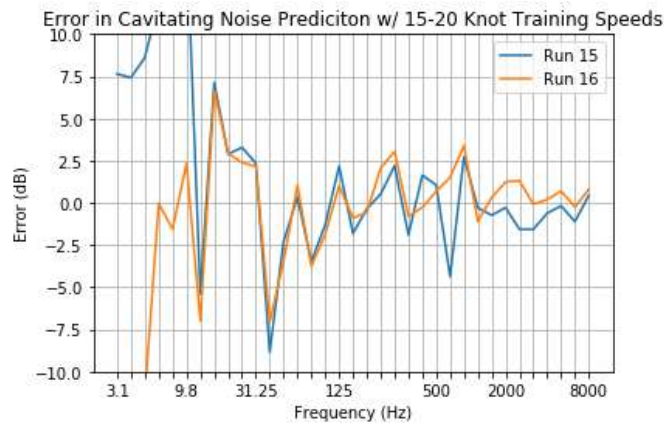


**Figure 28:** Error in 17 knot reconstruction using 15, 17, and 19 knot training runs. Y-axis reference is  $1\mu\text{Pa}^2/\text{Hz}$ .

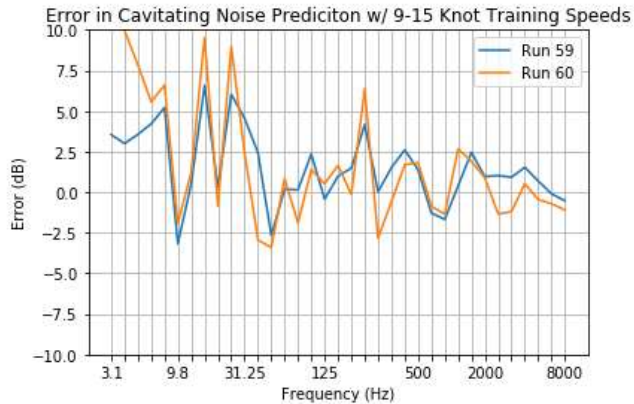


**Figure 29:** Error in 9 knot reconstruction using 9, 13, and 15 knot training runs. Y-axis reference is  $1\mu\text{Pa}^2/\text{Hz}$ .

The above error plots show that the error in the reconstructed spectra is reduced when the speeds are divided. In both cases, the maximum error in the reconstructed spectrum is around 5 dB for all frequency bins above 30 Hz. Interestingly, the error seems to improve as frequency increases in each case. Similar observations are made when reconstructing the other speeds associated with each matrix. This should be considered in the design of a signature management system, as the system will be more accurate if the cavitating speeds are divided up into smaller intervals. An ideal system would have a different matrix for each speed and machine state; however this is likely not feasible due to the large amount of ranging data that would be required for such a system.

#### 4.1.4 Reconstructing the 11 Knot Squeal

As mentioned in Section 3.4 staff on the trial noticed a squeal during 11 knot runs that was not present at other speeds. It is of interest to determine the source of this noise, and how much error this creates when attempting to reconstruct the spectrum using the matrix developed in the previous section with 9 knot, 13 knot, and 15 knot runs as training.

First, the spectrum for an 11 knot run was reconstructed using the same set of sensors that has been used for Machine State A runs throughout this Report: H1, H3, M2, M4, and M5. The resulting reconstruction is shown in Figure 30, along with the actual spectrum.

As expected, the reconstruction is reasonably accurate when predicting the 11 knot spectrum, save for the bin containing the 1443 Hz tone (and the previously mentioned problematic area below 50 Hz). A quick look at the spectrum from each of the sensors in this run shows why this is the case—the tone is only seen in the hull sensors on the starboard side, meaning it must be originating from the starboard propeller. Therefore, because only one of these sensors is included in the matrix in this test, the reconstruction does not fully account for this peak. A plot of the spectra for the hull sensors in this run is shown in Figure 31, for reference.

Interestingly, by replacing H1 with H4 so that both sensors that pick up the squeal are included in the correlation matrix, the reconstruction is able to very accurately show the peak from this tone. This reconstruction is shown in Figure 32.

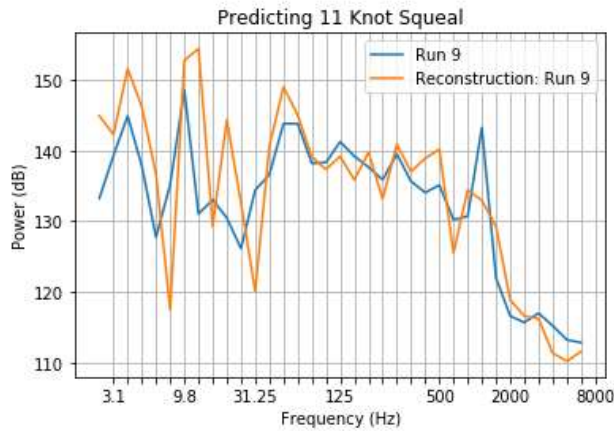


**Figure 30:** Eleven knot spectrum reconstruction from 9, 13 and 15 knot training runs. Y-axis reference is  $1\mu Pa^2/Hz$ .

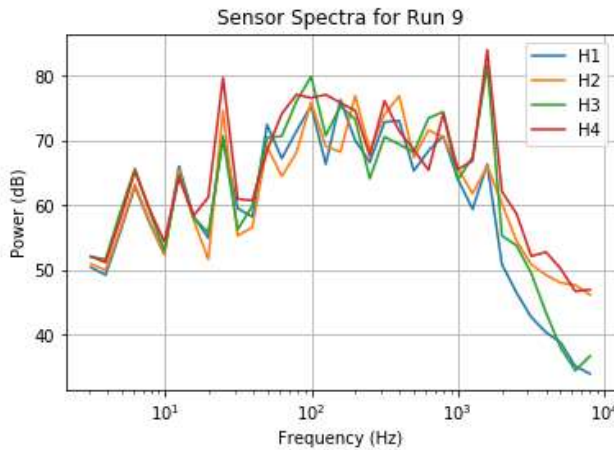


**Figure 31:** Hull sensor spectra for 11 knot run. Y-axis reference is  $1\mu Pa^2/Hz$ .

This finding leads to questions around which sensors should be included in the correlation. For tones that are seen predominantly on one side of the vessel, reconstruction may be more accurate if the sensors on the other side are not included. This, however, will sacrifice accuracy if any other unexpected tones are present. Therefore, in order to maintain the most consistency, it is still suggested that sensors from both sides of the vessel be included, as has been done throughout this Report. However, if costs permit, it may be beneficial to include more hull sensors in the system to increase the chance of unexpected vibrations being accounted for.

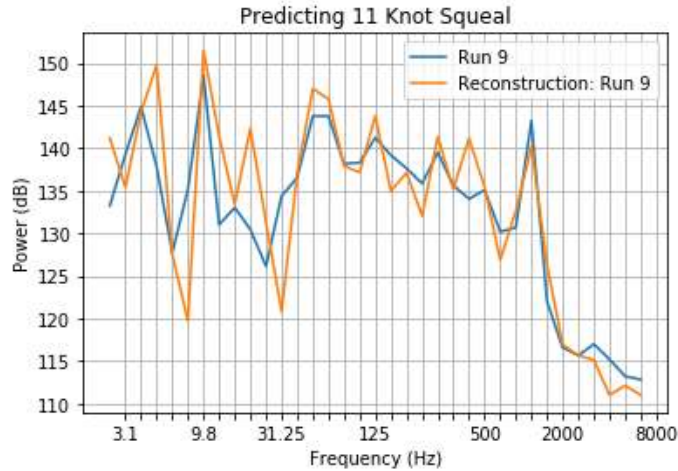


**Figure 32:** Eleven knot spectrum reconstruction when including both stbd sensors. Y-axis reference is  $1\mu\text{Pa}^2/\text{Hz}$ .

#### 4.1.5 Keel Runs

Four “keel runs” were recorded during the ORCA’s ranging session, where instead of sailing equidistantly between the two hydrophones, the ship sailed directly over one of them. This test will allow for an investigation into the differences between the near and far-field properties of the ship, something that is not yet fully understood.

To start, a simple comparison of the keel run spectra from each hydrophone was performed to verify that there was, in fact, a difference between the near-field and far-field spectra. In theory, the keel spectrum should be louder, as the ship is much closer. The result is displayed in Figure 33.

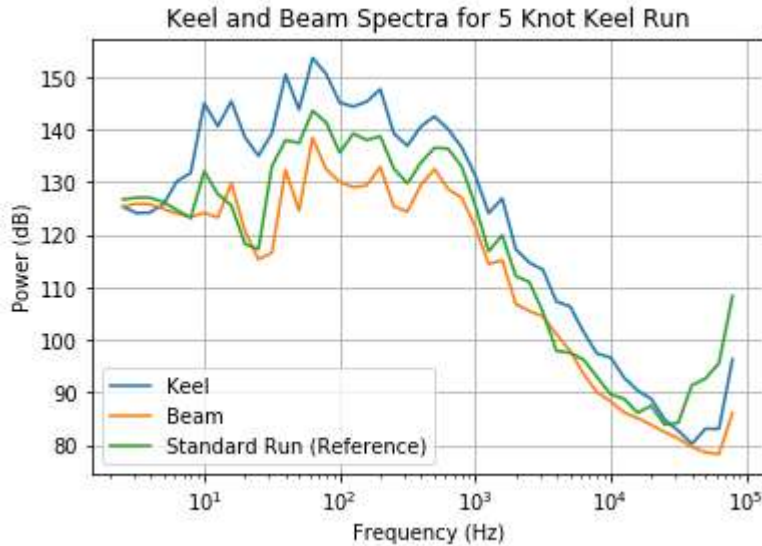


**Figure 33:** Keel vs. beam readings for keel runs. Y-axis reference is  $1\mu\text{Pa}^2/\text{Hz}$ .

The first thing that can be observed from this plot is the fact that the keel measurement is, in fact, louder than the beam measurement from the other hydrophone, as well as the levels from a normal 5 knot run included for reference. The beam measurement is also observed to be slightly quieter than the normal run. Much of the differences in these measurements could be attributed to the transmission loss ( $TL$ ) resulting from spherical spreading. An estimate of this loss can be calculated (from Reference [7]) through the following equation:

$$TL = 20 \cdot \log(R)$$

For a radius ( $R$ ) of 100m from the source, this results in a correction of approximately 41 dB, which has already been applied by the range to all hydrophone measurements in the preprocessing. Note that this is an approximation traditionally used by Canadian ranges, and the actual transmission loss from the ship to a hydrophone may differ. During a keel run, however, the radius becomes approximately 200 m for the far hydrophone and simply the depth of the closer hydrophone (26 m in the case of the North hydrophone). This results in necessary corrections of 46 dB and 26 dB respectively, as opposed to the 41 dB that had previously been applied by the range. Corrections of +5 dB and -15 dB were therefore applied to the far and near hydrophones respectively, producing the results in Figure 34.

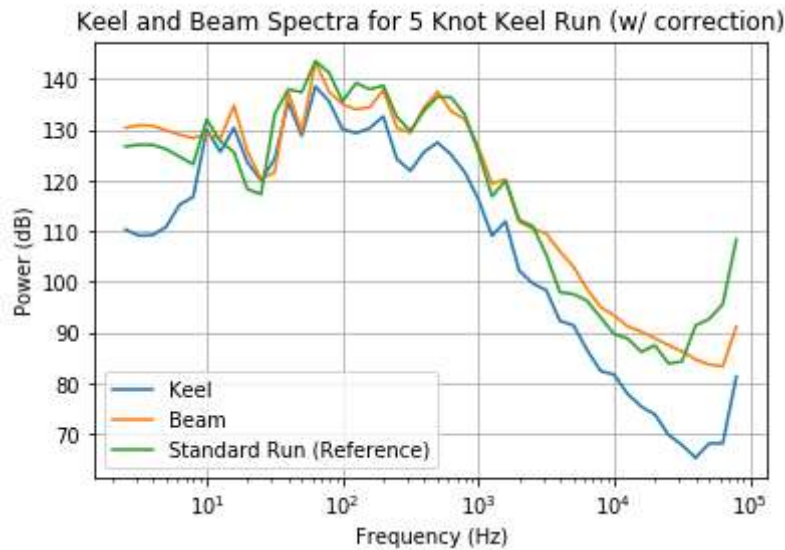


**Figure 34:** Keel vs. beam readings for keel runs after corrections. Y-axis reference is  $1\mu Pa^2/Hz$ .

Note that after this correction is applied, the beam measurement generally lines up with the expected spectrum. The keel run, however, is consistently between 5 and 10 dB lower than expected for frequencies above 100 Hz, and this difference becomes even more pronounced in frequencies above 10 kHz. This is of interest, as it means there is still a discrepancy between the properties of the ship's signature in the near field and that in the far field that is not completely understood. Note that it is recommended by the International Standards Organization [8] that the closest point of approach of the ship should be at least 100m to attempt to approximate the ship as a point source and to realize far-field conditions. This is not met in the keel run. As well, spherical spreading may not represent either the keel or beam runs accurately in this relatively shallow water (approximately 30 m). This should be studied further.

## 4.2 Cavitation Inception Prediction

The first step in predicting cavitation inception is to examine the noise level in each OTO bin as speed increases. By plotting the speed in the water against the vibration levels in the hull, we obtain plots such as those in Figures 35 and 36. Note that similar trends are seen in all hull sensors for bins above 100 Hz. Measurements from one hull sensor will be sufficient for this system.

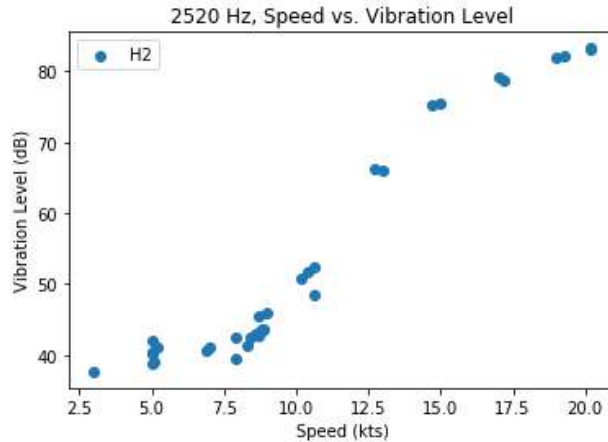


**Figure 35:** Speed vs. vibration level for the 2.52 kHz bin. Y-axis reference is  $1g^2/Hz$ .

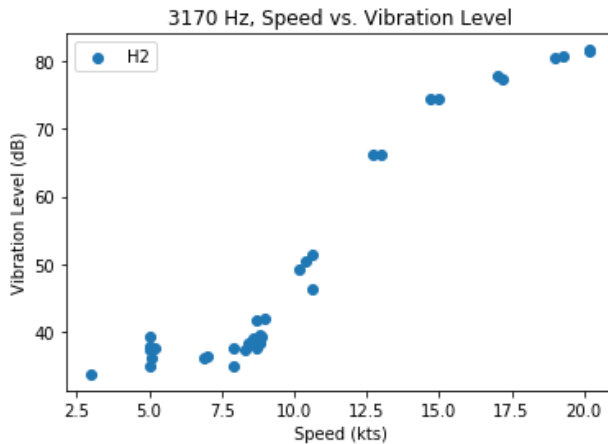


**Figure 36:** Speed vs. vibration level for the 3.17 kHz bin. Y-axis reference is  $1g^2/Hz$ .

Examination of the plots above shows a clear jump in vibration levels above 10 knots, which indicates that cavitation inception is somewhere below this speed. This matches the expected value of 8.5 knots noticed during the trial.

There is a baseline vibration level in many OTO bins for runs below cavitation. This level can be used to estimate the cavitation state. When a measurement is taken and converted to the frequency domain, it will be possible to compare this measurement to the baseline level in the bins that show the clearest trend, and determine if it is above the cavitation inception cut-off. The degree to which the measurement surpasses

the cut-off can be used to determine the certainty in the cavitation estimate, as well as the actual cavitation state. More sophisticated decision devices could be developed as well.

The more training data available at various speeds, the more precise the cut-off will be. Once a cavitation estimate is made, the result can be sent to the bridge through a simple light display that changes colour based on the cavitation state. Approximate cut-offs have been added to the plot in Figure 37 to provide a better idea of how they would look. In this case, accelerations below the yellow line would indicate “not likely cavitating” and above the red line “cavitating,” while between the two lines would be “possibly cavitating.”

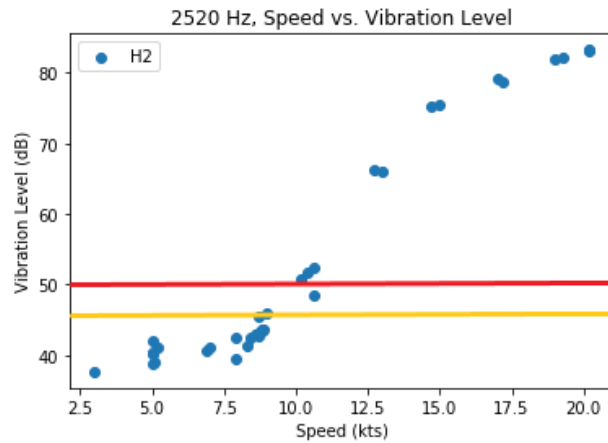


**Figure 37:** Approximate cavitation cut-offs for the 2520 Hz bin. Y-axis reference is  $1\mu Pa^2/Hz$ .

Due to redundancy, it is likely not necessary to compare every bin in the reconstructed spectrum to a unique threshold. Instead, the findings of this Report indicate that it would be better to use only the higher frequency bins for this prediction, as such frequencies showed a clearer trend between vibration level and speed. Therefore, not only will the use of a few higher-frequency bins reduce the complexity of the analysis, but it may actually produce a better, more accurate prediction of cavitation inception.

## 5 Conclusion

---

It has been demonstrated that it is possible to reconstruct the off-board noise spectrum of a ship using measured on-board vibrations with relatively good accuracy. While training and testing the system with the same speed and machine state, it was possible to predict the off-board spectrum to within 3 dB in each OTO bin over 30 Hz. By including a variety of speeds and machine states in the training runs, it is also possible to produce a more general correlation that can be applied to a variety of operating states of the ship. Due to the large difference in noise levels between lower and higher speeds, it is necessary to break up the speeds into smaller ranges and use a different correlation for each. It was shown that by breaking the speeds into 3 different ranges, significant improvement occurred in the estimated levels. Therefore, the system will likely require some sort of input to determine which relationship to use at any given time. Since any system should be able to know the GPS speed at any given moment, this should not be a problem.

It will also be possible to predict the cavitation state based on these measurements, as there is a clear trend in the vibration levels as the ship's speed changes. In this Report, a system was proposed that makes use of vibration thresholds around where cavitation is thought to occur in each bin to match the measured data to a cavitation state. Based on the proximity of the measurement to the threshold, it will be possible to determine with a certain degree of certainty whether the propeller is cavitating, and this information can be sent to the bridge through a simple light display.

In conclusion, this Report has shown that it is possible to create a signature management system for use in the civilian shipping industry using only a few accelerometers placed strategically around the engine room and on the hull near the propeller(s). Further work should be performed towards the development of software for such a program, and also towards applying this result to other, larger vessels.

## 6 Recommendations

---

Based on the results outlined in this Report, it is recommended that:

1. Further investigation be conducted into the improvement of reconstructions with different machine states, namely those with known sources. Different techniques should be considered to account for this added noise.
2. Different correlation methods be investigated to determine if the NNLS method is, in fact, the best option for this application.
3. A sample software program be built to demonstrate the cavitation prediction using existing ranging data from the ORCA trials.
4. The methods in this Report be applied to another ship, for example HCMS GLACE BAY, to determine if the results can be replicated across ships of varying sizes. Special interest should be taken with regards to whether the method proposed in this Report for cavitation prediction will also work on a larger ship, and how much ranging data is required for its design.
5. Further investigation be conducted into the discrepancies between near-field and far-field noise levels, and the implications this has for this and other projects.

## References

---

- [1] Gilroy, L., ORCA Underwater Noise Measurement Trial Plan, Defence Research and Development Canada, Reference Document, DRDC-RDDC-2020-D003, January 2020.
- [2] Mulders, I., Graafland, F., Bosschaart, C., van 't Hof, J., Acoustic Signature Estimation for MCDV HMCS Glace Bay, TNO report TNO 2018 R11656, The Netherlands, August 2018.
- [3] Virtanen, P. et al., SciPy 1.0: Fundamental Algorithms for Scientific Computing in Python. *Nature Methods*, 17(3), pp. 261–272, 2020.
- [4] Lawson C., Hanson R.J., Solving Least Squares Problems, Classics in Applied Mathematics, Volume 15, Society for Industrial and Applied Mathematics (SIAM), 1987.
- [5] Leggat, L.J., Propeller Cavitation Noise Investigations in a Free Field Environment, Defence Research Establishment Atlantic, DREA Technical Memorandum, DREA TM 82/E, 1982.
- [6] Hair, J.F., Ringle, C.M., Sarstedt, M., Editorial—Partial Least Squares Structural Equation Modeling: Rigorous Applications, Better Results and Higher Acceptance. *Long Range Planning*, 46(1–2), pp. 1–12, March 14, 2013.
- [7] Ross, D., Mechanics of Underwater Noise, Peninsula Publishing, Los Altos, CA, 1987.
- [8] ISO Underwater Acoustics Subcommittee, Underwater acoustics—Quantities and procedures for description and measurement of underwater sound from ships—Part 1: Requirements for precision measurements in deep water used for comparison purposes, ISO 17208-1, International Organization for Standardization, 2016.

## Annex A Dynamic Ranging Run List

*Table A.1: Dynamic ranging run list.*

Run Number	Identifier	Speed	Machinery State	Direction	Speed	Track Error (+N)
1	01PB03A01E	3	A	E	3.0	10.4
2	01PB03A01W	3	A	W	3.1	0.3
3	01PB05A01E	5	A	E	5.0	2.2
4	01PB05A01W	5	A	W	5.2	3.9
5	01PB07A01E	7	A	E	6.9	1.9
6	01PB07A01W	7	A	W	7.0	-7.0
7	01PB09A01E	9	A	E	8.6	2.1
8	01PB09A01W	9	A	W	9.0	-0.8
9	01PB11A01E	11	A	E	10.2	-1.7
10	01PB11A01W	11	A	W	10.6	-2.1
11	01PB13A01E	13	A	E	12.7	10.0
12	01PB13A01W	13	A	W	13.0	-2.7
13	01PB15A01E	15	A	E	14.7	6.0
14	01PB15A01W	15	A	W	15.0	-10.0
15	01PB17A01E	17	A	E	17.0	1.5
16	01PB17A01W	17	A	W	17.2	-7.7
17	01PB19A01E	19	A	E	19.0	-11.0
18	01PB19A01W	19	A	W	19.3	-10.4
19	01PB20A01E	20	A	E	20.2	-0.1
20	01PB20A01W	20	A	W	20.2	-7.0
21	01PB05B01E	5	B	E	5.0	-3.6
22	01PB05B01W	5	B	W	5.3	0.9
23	01PB11B01E	11	B	E	10.4	2.7
24	01PB11B01W	11	B	W	10.4	-0.2
25	02PB05C01E	5	C	E	4.9	7.1
26	02PB05C01W	5	C	W	5.2	-2.6
27	02PB05D01E	5	D	E	5.1	8.1
28	02PB05D01W	5	D	W	5.0	-0.1
29	02PB05E01E	5	E	E	5.0	2.3
30	02PB05E01W	5	E	W	5.1	0.6
31	02PB10E01E	11	E	E	10.4	10.0
32	02PB10E01W	11	E	W	10.4	-0.6
33	02PB15E01E	15	E	E	15.1	9.0

Run Number	Identifier	Speed	Machinery State	Direction	Speed	Track Error (+N)
34	02PB15E01W	15	E	W	15.0	-6.7
35	02PB05F01E	5	F	E	5.0	-3.0
36	02PB05F01W	5	F	W	5.0	0.3
37	02PB05G01E	5	G	E	5.6	8.8
38	02PB05G01W	5	G	W	5.4	5.0
39	02PB05H01E	5	H	E	5.6	-1.8
40	02PB05H01W	5	H	W	5.8	5.1
41	02PB03A02E	3	A	E	3.1	-3.3
42	02PB03A02W	3	A	W	3.1	2.6
43	02PB05A02E	5	A	E	5.0	-2.1
44	02PB05A02W	5	A	W	5.1	-4.6
63	03PB05A01K	5	A	Keel	5.0	4.0
64	03PB05A01K	5	A	Keel	5.0	2.0
65	03PB10A01K	11	A	Keel	10.2	4.8
66	03PB10A01K	11	A	Keel	10.4	0.7
45	02PB09A02E	9	A	E	8.7	6.3
46	02PB09A02W	9	A	W	8.9	1.8
47	02PB11A02E	11	A	E	10.4	2.5
48	02PB11A02W	11	A	W	10.6	-3.5
49	03PB17A02E	17	A	E	17.2	5.1
50	03PB17A02W	17	A	W	17.5	-5.6
51	03PB19A02E	19	A	E	19.4	4.1
52	03PB19A02W	19	A	W	19.6	-13.3
53	03PB05A03E	5	A	E	5.0	0.2
54	03PB05A03W	5	A	W	5.1	-1.5
55	03PB05A04E	5	A	E	5.0	3.8
56	03PB05A04W	5	A	W	5.0	8.2

## Annex B Results From Attempted Reconstructions

*Table B.1: Results from attempted reconstructions.*

Sensors Used	Training Speed	Test Speed	Training Machine State	Test Machine State	Training Runs	Test Runs	Average Error	Max Error
H1, H3	5	5	A	A	53, 54, 55, 56	3, 4, 43, 44	2.68	15.1
H2, H4	5	5	A	A	53, 54, 55, 56	3, 4, 43, 44	2.9	14.3
H1, H2, H3, H4	5	5	A	A	53, 54, 55, 56	3, 4, 43, 44	2.63	15.9
H1, H3, M2	5	5	A	A	53, 54, 55, 56, 4	3, 43, 44	1.89	5.4
H1, H3, M7	5	5	A	A	53, 54, 55, 56, 4	3, 43, 44	2.2	10.5
H1, H3, M5	5	5	A	A	53, 54, 55, 56, 4	3, 43, 44	1.49	5.28
H1, H3, M4, M5	5	5	A	A	53, 54, 55, 56, 4	3, 43, 44	1.31	4.45
H1, H3, M2, M4, M5	5	5	A	A	53, 54, 55, 56, 4	3, 43, 44	1.45	3.41
H1, H3	9	9	A	A	7, 8, 45, 46, 57, 58	59, 60	1.59	6.18
H2, H4	9	9	A	A	7, 8, 45, 46, 57, 58	59, 60	1.71	4.82
H1, H2, H3, H4	9	9	A	A	7, 8, 45, 46, 57, 58	59, 60	1.43	4.82

Sensors Used	Training Speed	Test Speed	Training Machine State	Test Machine State	Training Runs	Test Runs	Average Error	Max Error
<b>H1, H3, M2</b>	9	9	A	A	7, 8, 45, 46, 57, 58	59, 60	1.68	5.1
<b>H1, H3, M7</b>	9	9	A	A	7, 8, 45, 46, 57, 58	59, 60	1.62	4.82
<b>H1, H3, M5</b>	9	9	A	A	7, 8, 45, 46, 57, 58	59, 60	1.21	4.39
<b>H1, H3, M4, M5</b>	9	9	A	A	7, 8, 45, 46, 57, 58	59, 60	1.19	4.27
<b>H1, H3, M2, M4, M5</b>	9	9	A	A	7, 8, 45, 46, 57, 58	59, 60	1.45	4.27
<b>H1, H3</b>	19	19	A	A	17, 18, 61, 62, 51	51, 52	1.27	4.7
<b>H2, H4</b>	19	19	A	A	17, 18, 61, 62, 51	51, 52	1.23	5.17
<b>H1, H2, H3, H4</b>	19	19	A	A	17, 18, 61, 62, 51	51, 52	1.19	5.2
<b>H1, H3, M2</b>	19	19	A	A	17, 18, 61, 62, 51	51, 52	1.17	4.68
<b>H1, H3, M7</b>	19	19	A	A	17, 18, 61, 62, 51	51, 52	0.95	3.45
<b>H1, H3, M5</b>	19	19	A	A	17, 18, 61, 62, 51	51, 52	1.23	3.49
<b>H1, H3, M4, M5</b>	19	19	A	A	17, 18, 61, 62, 51	51, 52	1.08	4.1

Sensors Used	Training Speed	Test Speed	Training Machine State	Test Machine State	Training Runs	Test Runs	Average Error	Max Error
<b>H1, H3, M2, M4, M5</b>	19	19	A	A	17, 18, 61, 62, 51	51, 52	0.97	4.4
<b>H2, H4, M2, M4, M5, M6, M7, M8</b>	5	5	A	B, C, D, E, F, G, H	3, 4, 43, 44, 53, 54, 55, 56	54, 21, 25, 27, 29, 35, 37, 39	4.2	23.98
<b>H2, H4, M2, M4, M5, M6, M7, M8</b>	5	5	A, B, C, D, E, F, G, H	A, B, C, D, E, F, G, H	3, 4, 43, 44, 53, 54, 55, 56	54, 21, 25, 27, 29, 35, 37, 39	2.02	9.33
<b>H1, H3, M2, M4, M5</b>	5, 7	5	A	A	3, 4, 5, 6, 53, 54	55, 56	1.86	6.34
<b>H1, H3, M2, M4, M5</b>	9, 13, 15	9	A	A	7, 8, 11, 12, 13, 14, 57, 58	59, 60	2.53	6.37
<b>H1, H3, M2, M4, M5</b>	15, 17, 19, 20	19	A	A	15, 16, 17, 18, 19, 20, 51, 52	61, 62	1.85	6.41

## List of Symbols/Abbreviations/Acronyms/Initialisms

---

$C$	weighting matrix
CFB	Canadian Forces Base
DRDC	Defence Research and Development Canada
FMF	Fleet Maintenance Facility
$h$	hydrophone spectral power
NB	narrow band
NNLS	non-negative least squares
OTO	one third octave
PCT	patrol craft training
$R$	radius
RCN	Royal Canadian Navy
$s$	accelerometer spectral power
$\omega$	weighting value

**DOCUMENT CONTROL DATA**

\*Security markings for the title, authors, abstract and keywords must be entered when the document is sensitive

1. ORIGINATOR (Name and address of the organization preparing the document. A DRDC Centre sponsoring a contractor's report, or tasking agency, is entered in Section 8.)  DRDC – Atlantic Research Centre Defence Research and Development Canada 9 Grove Street P.O. Box 1012 Dartmouth, Nova Scotia B2Y 3Z7 Canada	2a. SECURITY MARKING (Overall security marking of the document including special supplemental markings if applicable.)  <b>CAN UNCLASSIFIED</b>
	2b. CONTROLLED GOODS  <b>NON-CONTROLLED GOODS  DMC A</b>
3. TITLE (The document title and sub-title as indicated on the title page.)  <b>Results from off-board noise prediction study in ORCA-class training vessel</b>	
4. AUTHORS (Last name, followed by initials – ranks, titles, etc., not to be used)  <b>Larsen, G.; Dupuis, J.; Gilroy, L.</b>	
5. DATE OF PUBLICATION (Month and year of publication of document.)  <b>January 2021</b>	6a. NO. OF PAGES (Total pages, including Annexes, excluding DCD, covering and verso pages.)  <b>44</b>
	6b. NO. OF REFS (Total references cited.)  <b>8</b>
7. DOCUMENT CATEGORY (e.g., Scientific Report, Contract Report, Scientific Letter.)  <b>Scientific Report</b>	
8. SPONSORING CENTRE (The name and address of the department project office or laboratory sponsoring the research and development.)  DRDC – Atlantic Research Centre Defence Research and Development Canada 9 Grove Street P.O. Box 1012 Dartmouth, Nova Scotia B2Y 3Z7 Canada	
9a. PROJECT OR GRANT NO. (If appropriate, the applicable research and development project or grant number under which the document was written. Please specify whether project or grant.)  <b>01ec</b>	9b. CONTRACT NO. (If appropriate, the applicable number under which the document was written.)
10a. DRDC PUBLICATION NUMBER (The official document number by which the document is identified by the originating activity. This number must be unique to this document.)  <b>DRDC-RDDC-2021-R003</b>	10b. OTHER DOCUMENT NO(s). (Any other numbers which may be assigned this document either by the originator or by the sponsor.)
11a. FUTURE DISTRIBUTION WITHIN CANADA (Approval for further dissemination of the document. Security classification must also be considered.)  <b>Public release</b>	
11b. FUTURE DISTRIBUTION OUTSIDE CANADA (Approval for further dissemination of the document. Security classification must also be considered.)	
12. KEYWORDS, DESCRIPTORS or IDENTIFIERS (Use semi-colon as a delimiter.)  <b>Naval Acoustic Signature Management; Acoustics; Transfer Function; Cavitation</b>	

13. ABSTRACT (When available in the document, the French version of the abstract must be included here.)

Transport Canada is interested in the real-time estimation of underwater radiated noise based on on-board measurements due to its impact on marine mammals. At Transport Canada's request, Defence Research and Development Canada (DRDC) performed a trial to measure both on-board vibrations and off-board underwater noise produced by an ORCA-class patrol vessel. The post-trial work is a first attempt at adapting real-time acoustic signature estimation procedures that have previously been developed by an international partner (COSIMAR, STEAM and MEASURE trials). Analysis of the trial data shows that it is possible to accurately reconstruct the off-board noise spectrum using few hull and machine-mounted accelerometers. It should also be possible to estimate the cavitation state of the propeller based on the predicted noise levels.

Transports Canada songe à évaluer en temps réel le bruit sous-marin en mesurant les vibrations à bord des navires en raison de leurs effets sur les mammifères marins. À la demande de Transports Canada, Recherche et développement pour la défense Canada (RRDC) a procédé à un essai afin de mesurer les vibrations à bord et le bruit sous-marin produit par un navire de patrouille de la classe ORCA. Les travaux effectués après cet essai constituent une première tentative pour adapter la procédure d'évaluation de la signature acoustique en temps réel élaborée précédemment par un partenaire international (essais de COSIMAR, STEAM et MEASURE). L'analyse des données de l'essai a montré qu'il était possible de reproduire avec exactitude le spectre du bruit sous-marin à l'aide de quelques accéléromètres montés sur la coque et embarqués sur la machine. On devrait également être en mesure d'évaluer l'état de cavitation de l'hélice sur la base des niveaux de bruit prévus.